SIMULATION OF RADIAL TEMPERATURE FIELD OF OVERHEAD CONDUCTORS ON QINGHAI-TIBET PLATEAU

ZHANG Hongwei*, LIU Yongdou*,**, HAN Zhilei*, LUO Junpeng***, LIU Shengkun*
*School of Civil Engineering and Water Resources, Qinghai University, Xining 810016, China,
** Qinghai Provincial Key Laboratory of Building Energy-saving Materials and Engineering Safety, Xining ,810016, China,
***Provincial Demonstration Center for Experimental Fundamental Mechanics Education at Qinghai University
E-mails: hongggzz@163.com, liu_yongdou@qhu.edu.cn

ABSTRACT

The temperature field variation of overhead conductors in the operating environment of the Qinghai-Tibet Plateau is significant, causing the stress on the conductor wires to fluctuate with climate changes, leading to fatigue and wire breakage. Conducting numerical simulation and analysis of the temperature field of overhead conductors in this environment is crucial for enhancing the safety of transmission lines. This paper establishes a numerical algorithm for solving the radial temperature distribution of overhead conductors in operation based on the two-dimensional steady-state heat balance theory. This method is applied to the numerical simulation of the temperature field of the heat-resistant aluminum alloy conductor NRLH58GJ630-55 in the Qinghai-Tibet Plateau environment, analyzing the effects of current load, wind speed, and ambient temperature on the radial temperature distribution of the overhead conductor.

Key words: *transmission conductors, radial temperature, two-dimensional steady-state thermal equilibrium, finite element, numerical simulation*

1. INTRODUCTION

The climate conditions on the Qinghai-Tibet Plateau are uniquely complex and highly variable, characterized by significant diurnal temperature variations. For example, in Xining, Qinghai Province, the annual maximum temperature can reach 33.7°C, while the minimum temperature can drop to -19.6°C. Wind speeds can reach up to 15.1 $m \cdot s^{-1}$, classified as a strong gale [1]. These factors lead to substantial and frequent changes in the temperature field of overhead conductors operating in the Qinghai-Tibet Plateau. This results in significant variations in the sag and tensile stress of transmission lines, potentially causing incidents such as tree contact discharges [2,3] and conductor fatigue failure [4-6]. The power network on the Qinghai-Tibet Plateau is a crucial part of the national "West-to-East Power Transmission" project and is vital for local residential and economic development. The harsh climate conditions on the plateau pose severe challenges to the performance and reliability of overhead conductors. Therefore, numerically simulating the radial temperature distribution of overhead conductors in the Qinghai-Tibet Plateau operational environment and studying the impact of environmental changes on their temperature field are of great significance for improving the safety and reliability of overhead conductors.

Liu Gang et al. [7] considered the thermal conduction effect of air gaps in overhead conductors, establishing an electromagnetic-thermal coupling model. They conducted a finite element analysis of the temperature distribution and radial temperature difference of overhead conductors and experimentally verified the specific variations in the steady-state radial temperature difference of steel-cored aluminum stranded wires under natural convection conditions. Dong Xuanchang et al. [8] developed a thermal circuit model based on the internal conductor structure of overhead conductors to improve the accuracy of predicting temperature distribution under convection conditions, enhancing the reliability of the transmission system. Zhang Meng et al. [9] studied the impact of radial temperature differences on the allowable current-carrying capacity by considering air gaps and actual contact conditions between conductor strands, providing a reference for optimizing transmission line load capacity. Li Junhui et al. [10] focused on enhancing the dynamic capacity and transmission capability of overhead transmission lines. They innovatively established an electromagnetic coupling finite element shunt model to more accurately calculate the radial temperature distribution of transmission lines, thereby safely and efficiently increasing the load-bearing capacity of the lines. Ľ. Beňa et al. [11] considered the corona effect in the numerical calculation of the operating temperature of overhead conductors, analyzing the power loss caused by the corona effect, thereby improving the calculation accuracy of the operating temperature of overhead conductors under actual conditions. Liu Zhilü et al. [12] mainly analyzed the radial temperature field distribution of overhead conductors by establishing a three-dimensional finite element simulation model. They found significant differences in temperature distribution under different cooling conditions, emphasizing the impact of axial heat transfer. Cui Jiayue et al. [13] determined the temperature variation patterns of damaged conductors through tests on LGJ/240-30 conductors. They established a damaged conductor model combined with finite element simulation to calculate the local temperature characteristics of damaged conductors, applicable to real-time monitoring of conductor fatigue damage states. Existing methods for calculating the radial temperature distribution of overhead conductors have not sufficiently considered the porosity between conductor strands and the heat exchange coefficient between conductor strands and the surrounding air. Moreover, these methods have not accounted for the unique regional characteristics and the harsh operational conditions of overhead conductors on the Qinghai-Tibet Plateau.

This paper comprehensively considers factors such as current, solar radiation, convection, and radiative cooling,

applying the two-dimensional steady-state thermal equilibrium theory to develop a numerical solution algorithm for simulating the radial temperature distribution of transmission conductors under the Qinghai-Tibet Plateau environment. Using the heat-resistant aluminum alloy conductor NRLH58GJ630-55 as an example, the effects of current-carrying capacity, wind speed, and ambient temperature conditions on the radial temperature distribution of the conductor under different convection conditions are studied. This method is expected to provide accurate temperature distribution information, thereby offering reliable data support for fatigue and clearance control of power transmission systems operating on the Qinghai-Tibet Plateau.

2. NUMERICAL SOLUTION METHOD FOR THE TEMPERATURE FIELD OF OVERHEAD CONDUCTORS

2.1. Two-Dimensional Steady-State Thermal Equation

Due to the counter-wound characteristics of overhead conductors, the three-dimensional finite element modeling, particularly of the void regions, presents significant challenges. Furthermore, considering that the cross-sectional geometry of overhead conductors remains largely uniform along their length, this study neglects any temperature distribution variations in the longitudinal direction. The temperature field of the overhead conductor can be established and solved through the two-dimensional thermal equilibrium equation on its cross-section [14].

$$k(T''_{xx} + T''_{yy}) + \eta = 0, (x, y) \in \Omega \tag{1}$$

In equation (1) and (2): T represents the two-dimensional temperature distribution of the conductor cross-section. In the equation, $T''_{xx}, T''_{yy}, T'_x, T'_y$ denote the second-order and first-order derivatives of T with respect to the coordinates x and y, respectively. The symbol k represents the thermal conductivity, which varies for the metal and air regions, assuming they are homogeneous and isotropic materials. Different values are assigned for the steel core, aluminum strands, and air regions. The symbol η represents the volumetric heat generation rate, which varies across the steel core, aluminum strands, and air regions, with the air region being zero.

The heat balance equation at the boundary of the conductor is given by

$$q_n = -k(T'_x n_x + T'_y n_y) = \alpha(T_{sur} - T_a), (x, y) \in \Gamma \tag{2}$$

The term q_n denotes the heat flux along the normal direction n on the conductor surface. T_{sur} and T_a are the boundary temperature of the conductor and the ambient temperature, respectively. The symbol α represents the composite heat transfer coefficient.

By applying the principle of virtual work to integrate by parts equation (1) and incorporating equation (2) as a boundary condition into the integrated heat balance equation, we obtain:

$$\begin{aligned} &\int_\Omega k(\delta T'_x T'_x + \delta T'_y T'_y)\,\mathrm{d}\Omega + \int_\Gamma \delta T \alpha T_{sur}\,\mathrm{d}\Gamma \\ &= \int_\Gamma \delta T \alpha T_a\,\mathrm{d}\Gamma + \int_\Omega \delta T \eta\,\mathrm{d}\Omega \end{aligned} \tag{3}$$

By applying equation (3) and interpolating the temperature field shape functions within the cross-section of the overhead conductor (including the steel core, aluminum strands, and air regions), the temperature values at each finite element node can be obtained.

2.2. Heat Source and Heat Dissipation Calculation

Considering the high current-carrying capacity and stability of steel-cored aluminum stranded wires [15], this paper studies the temperature field distribution using the heat-resistant steel-cored aluminum stranded wire NRLH58GJ630-55 as an example. Its cross-sectional structure is shown in Fig. 1, where the outer layer consists of aluminum conductors, and the inner layer is made of steel core material.

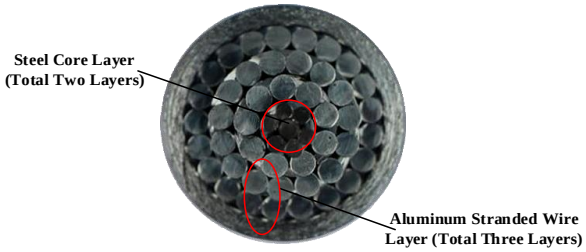

Fig. 1 Cross-Section of Steel-Core Aluminum Stranded Conductor

The heat source analysis of the steel-cored aluminum stranded wire is as follows: the outermost layer of aluminum wires, in addition to Joule heating, also absorbs solar radiation, making its heat source a combination of Joule heat and solar heat radiation. The inner aluminum wires and the steel core cannot receive solar radiation, so their heat source is solely from Joule heating. The heat power generated in the overhead conductor due to Joule heating can be determined by the conductor's direct current, average temperature, and composite resistivity [20]:

$$P_J = I_{dc}^2 R_{dc}\left[1 + \alpha_{20}\left(T_{av} - 20\right)\right] \tag{4}$$

It should be noted that P_J is the heat power generated by the conductor; T_{av} is the average temperature of the conductor; α_{20} is the resistivity coefficient of the conductor at room temperature (20°C), which does not vary significantly with different models of steel-cored aluminum stranded wires and is approximately 3.6‰; R_{dc} is the total resistance of the stranded wire; I_{dc} and I_{ac} is the direct current, which can be converted to alternating current:

$$I_{dc} = I_{ac}\sqrt{1.0123 + 2.36 \times 2.36 \times 10^{-5} I_{ac}} \tag{5}$$

Note that the above formula is based on results of

measurements on stranded conductors [22]. These values were obtained from empirical measurements and data fitting.

The solar radiation heat power is given by:

$$P_s = \gamma QD \tag{6}$$

In the equation (6): Q represents the solar radiation intensity; D is the total diameter of the conductor; and γ denotes the absorption rate of the conductor to sunlight, which is typically set to 0.50 under standard conditions.

In the equation (2), k represents the thermal conductivity, denoted as k_{al} in the aluminum strands region, k_{st} in the steel core region, and k_{air} in the air region. Both k_{al} and k_{st} are related to the temperature field, and k_{air} is also temperature-dependent, with their relationships defined as follows:

$$k_{air} = 2.42\times10^{-2} + 7.2\times10^{-5}T_{av} \tag{7}$$

In the equation (7): T_{av} represents the average temperature of the cross section. These values, 2.42×10^{-2} W/m·K and 7.2×10^{-5} W/m·K^2, were obtained from empirical measurements and data fitting.

In a unit length of the conductor, the steel core and aluminum strands are connected in parallel with the same voltage, while the current is inversely proportional to the resistance, and the resistance is inversely proportional to the cross-sectional area and directly proportional to the resistivity [16]. Based on these proportional relationships, the ratio of the current in the steel core I_{st} to the current in the aluminum strands I_{al} can be derived

$$\lambda = \frac{I_{st}}{I_{al}} = \frac{A_{st}}{A_{al}} \cdot \frac{\rho_{al}}{\rho_{st}} \tag{8}$$

A_{al} and A_{st} in this represent the total cross-sectional areas of the aluminum strands and the steel core, respectively; ρ_{al} and ρ_{st} are the resistivities of the aluminum strands and steel core, respectively. Further analysis shows that for the same section of the internal wire, the voltage across the steel core and aluminum strands is the same, and Joule heat is proportional to the current. Therefore, the volumetric heat generation rates for the inner aluminum wires and the steel core can be expressed by equations (9) and (10).

$$\eta_{al} = \frac{P_J}{(\lambda+1)A_{al}} \tag{9}$$

$$\eta_{st} = \frac{P_J\lambda}{(\lambda+1)A_{st}} \tag{10}$$

For the outer aluminum strands, the heat analysis must additionally consider the thermal effect of solar radiation. This means that their volumetric heat generation rate includes not only internal factors but also the heat from solar radiation. Thus, the volumetric heat generation rate is given by:

$$\eta'_{al} = \frac{P_J}{(\lambda+1)A_{al}} + \frac{\gamma QD}{A_{al}} \tag{11}$$

The above outlines the heat sources for the overhead conductor.

Typically, the heat dissipation for overhead conductors involves convective and radiative cooling [17]. For the unit length of the steel-cored aluminum stranded wire, following the principle of constant volumetric heat dissipation rate [10]:

$$P_c + P_r = q_n A \tag{12}$$

Where: P_c and P_r represent the convective and radiative heat dissipation power, respectively; A is the lateral surface area per unit length of the aluminum strands.

Thus, the composite heat transfer coefficient α in equation (2) for the conductor surface can be determined as follows:

$$\alpha = \frac{P_c + P_r}{(T_{sur} - T_a)A} \tag{13}$$

2.3. Radial Temperature Field Numerical Calculation Process

From the weak form of the thermal equilibrium equation for the temperature field (3), it is known that key parameters include the thermal conductivity k, the composite heat transfer coefficient α, and the volumetric heat generation rate η, all of which are crucial for solving the equation. Research indicates that the thermal conductivity of air k_{air} is related to the average temperature of the conductor T_{av}. The volumetric heat generation rates of the steel core and aluminum strands are also related to the average temperature, as shown in equations (4) and (9) -(11). According to equation (13), the composite heat transfer coefficient α is related to the average temperature of the conductor's outer surface. Therefore, the set of equations discretized from equation (3) is a nonlinear function of the temperature field and requires iterative solving.

This study employs the fixed-point iteration method [18, 19] to solve the radial temperature field of the overhead line. The proposed method has been validated through a series of experiments [20], demonstrating its reliability in various situations. The numerical iteration process is as follows (Fig. 2).

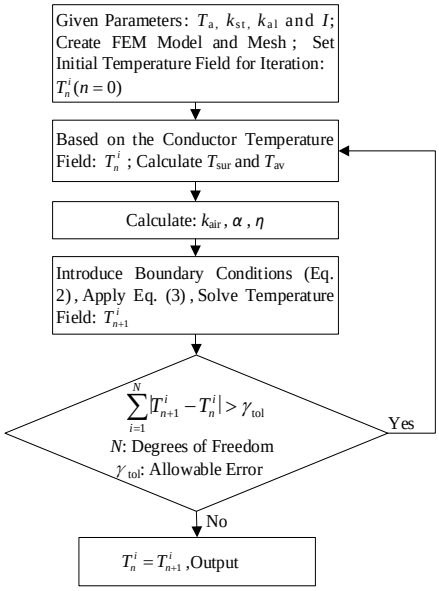

Fig. 2 Numerical Calculation Process Flowchart

3. RADIAL TEMPERATURE FIELD IN QINGHAI-TIBET PLATEAU

3.1. Finite Element Modeling of Overhead Conductors

This study examines the temperature field distribution of the NRLH58GJ630-55 heat-resistant aluminum conductor steel-reinforced (ACSR). The geometric parameters of this conductor are listed in, and its cross-section is shown in Fig. 3(a). The corresponding finite element model is illustrated in Fig. 3(b). This study uses triangular elements with a maximum mesh size of 0.3 mm, comprising a total of 19,515 elements and 10,187 nodes.

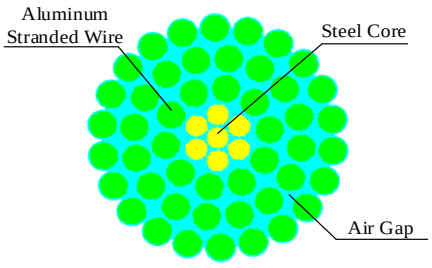

(a) Cross-Section of the Conductor

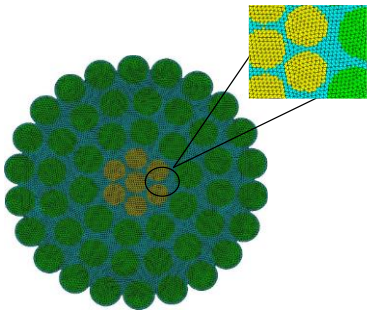

(b) Finite Element Model Diagram

Fig. 3 NRLH58GJ630-55 Steel-Core Heat-Resistant Aluminum Stranded Conductor

3.2. Influence of Current Load on Radial Temperature Distribution of Overhead Conductors

To investigate the radial temperature field distribution of an energized conductor, the heat-resistant steel-cored aluminum stranded wire NRLH58GJ630-55 was selected as the study example. The radial temperature field was examined under an AC current of 600A (rated current). The basic parameters of the NRLH58GJ630-55 conductor are as follows: the resistivity of the steel core and aluminum strands are ρst = 20×10-8 Ω·m and ρal = 3.253×10-8 Ω·m, respectively; the thermal conductivity coefficients are kst =80 W/m·K for the steel core and kal = 237 W/m·K for the aluminum strands. The solar irradiance was taken as the annual average intensity in Xining, Q = 184.05 W/m2 [23], and the ambient temperature was taken as the annual average temperature in Xining, 6.6℃ [24, 25]. Using the numerical method described in Section 2.3, the radial temperature distribution of the NRLH58GJ630-55 conductor was obtained under the condition of a wind speed of 0 m·s-1 (natural convection) and a current of 600 A. These temperature distribution results are shown in Figure 4. From the calculated results, the following observations can be made: 1) The temperature deviation of the strands in the same layer is minimal and can be ignored; 2) Overall, the temperature of the overhead conductor shows a trend of being higher inside and lower outside. The average temperatures of the strands in each layer are shown in Table 2, with the temperature difference between the innermost and outermost layers reaching up to 6.15℃. The temperature distribution characteristics of the overhead conductor can be explained as follows: 1) The heat sources and heat dissipation paths for the strands in the same layer are basically the same, resulting in minimal temperature deviation; 2) Compared to the outer strands, the heat of the inner strands is less likely to diffuse outward, leading to higher temperatures in the inner strands. The thermal conductivity coefficient of the air gaps within the overhead conductor is very small, resulting in a significant temperature difference between the inner and outer layers.

To gain a deeper understanding of the radial temperature variation of overhead conductors with changing current, this study calculated the impact of current variations in the range of 100 A to 800 A (in increments of 100 A) on the radial temperature. The temperature patterns of the innermost and outermost layers of the overhead conductor under different currents are discussed, as shown in Fig. 2. To fully consider the effects of convection conditions, calculations were conducted under the following two convection conditions: natural convection with no wind (ideal conditions) and forced convection with an average annual wind speed of v_w = 2.6 m·s^{-1} and wind direction δ = 90° [24, 25]. Figure 5 shows that under both convection conditions, the temperatures of the innermost and outermost layers increase non-linearly with the increase in current. When the current increases from 100 A to 800 A, under natural convection, the temperatures of the innermost and outermost layers of the overhead conductor increase from 10.85℃ to 40.21℃ and from 9.81℃ to 29.7℃, respectively. Under forced convection, the temperatures of the innermost and outermost layers increase from 8.34℃ to 23.26℃ and from 7.31℃ to 13.37℃, respectively. The temperatures under forced

Table 1 NRLH58GJ630-55 Conductors specifications

Standard Cross-Sectional Area/mm²		Number		Diameter /mm		Cross-sectional area /mm		Outer diameter /mm	Breaking Force /kN
aluminum	steel	aluminum	steel	aluminum	steel	aluminum	steel		
630	55	48	7	4.12	3.20	639.92	56.30	34.32	164.31

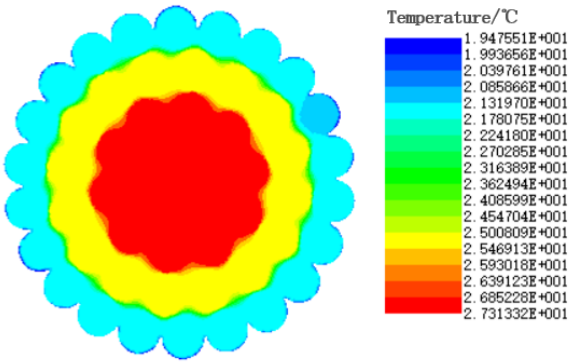

Fig. 4 Radial Temperature Distribution of NRLH58GJ630-55 Conductor under Natural Convection

Table 2 Temperature of Different Layers in Cross-Section

Layer number	Average temperature/℃
1	27.31317
2	27.30395
3	27.13806
4	24.96927
5	21.16677

convection are significantly lower than those under natural convection for the same current, and the difference between the two increases with the current.

The fitting results of the calculation indicate the following functional relationship between the innermost layer temperature of the overhead conductor and the current:

$$Y_t = A + BX_c + CX_c^2 \tag{14}$$

Where X_c represents the current, and Y_t represents the radial temperature of the overhead conductor. The fitting coefficients under natural convection conditions are as follows: A = (10.249 ± 0.023) ℃, B = (1.51 ± 0.15)×10^{-3} ℃/A, C = (4.491 ± 0.025)×10^{-5} ℃/A^2; similarly, the fitting coefficients under forced convection conditions are expressed as follows: A' = (8.243 ± 0.046) ℃, $B`$ = (-1.18 ± 0.24)×10$^{-3}$ ℃/A, $C`$ = (2.536 ± 0.026)×10^{-5} ℃/A^2.

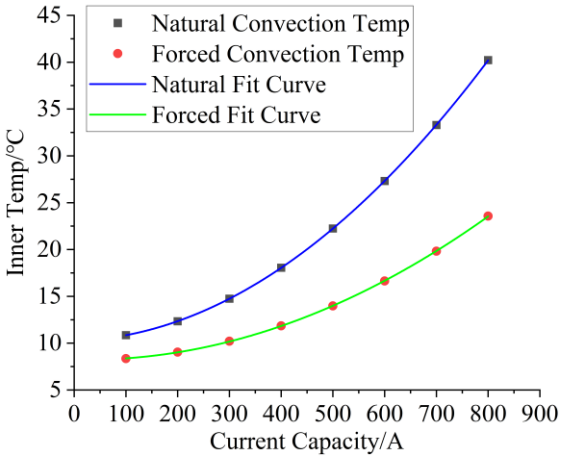

(a) Innermost Layer Temperature

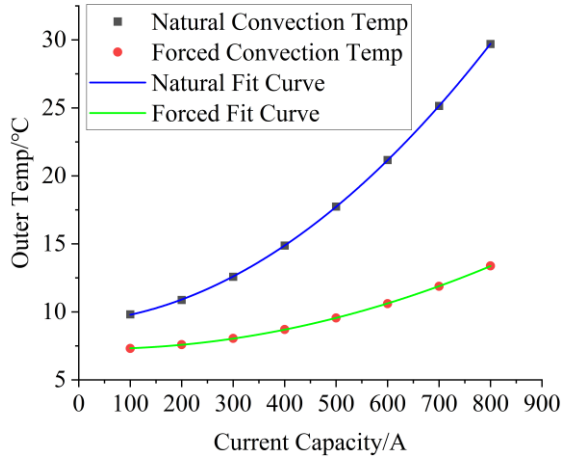

(b) Outermost Layer Temperature

Fig. 5 Inner and Outer Layer Temperature Variation of NRLH58GJ630-55 Conductor with Load

3.3. Influence of Wind Speed on Radial Temperature Distribution of Overhead Conductors

To study the impact of wind speed on the radial temperature field of overhead conductors, the wind speed range of 0 - 15.1 m·s^{-1} was selected based on the wind speed variation in Xining, Qinghai Province, in 2021, while keeping other parameters constant [25]. The radial temperature distribution of the heat-resistant steel-cored

aluminum stranded wire NRLH58GJ630-55 was obtained, as shown in Fig. 6. The results indicate the following:

1) As wind speed increases, the temperatures of both the innermost and outermost layers of the overhead conductor gradually decrease, exhibiting a nonlinear functional relationship with wind speed. The fitted curve expression is given in Equation (14).

2) With the increase in wind speed, the rate of temperature decrease for both the innermost and outermost layers of the overhead conductor slows down. The decrease rate significantly reduces when the wind speed exceeds 4.5 $m \cdot s^{-1}$. The reasons for these phenomena can be summarized as follows:

1) Increasing wind speed enhances the convective heat transfer between the air and the surface of the overhead conductor, resulting in a decrease in the radial temperature of the conductor.

2) When wind speed is low, an increase in wind speed causes the primary heat dissipation mode of the conductor's outer surface to shift from radiation to convection. During this phase, wind speed significantly impacts the temperatures of both the innermost and outermost layers. However, once the wind speed exceeds 4.5 $m \cdot s^{-1}$, further increases do not change the heat dissipation mode, resulting in a lesser impact on the radial temperature of the overhead conductor.

Fitting Formulas for Inner and Outer Layer Temperatures with Wind Speed:

$$Y_t = AX^B \tag{15}$$

Where X is wind speed ($m \cdot s^{-1}$), The fitting coefficients for the outer layer: A = (12.84 ± 0.26) $℃(m \cdot s^{-1})^{-B}$, B = (-0.185 ± 0.011); The fitting coefficients for the inner layer: $A`$ = (18.74 ± 0.28) $℃ \cdot (m \cdot s^{-1})^{-B`}$, $B`$ = (-0.1139 ± 0.0076).

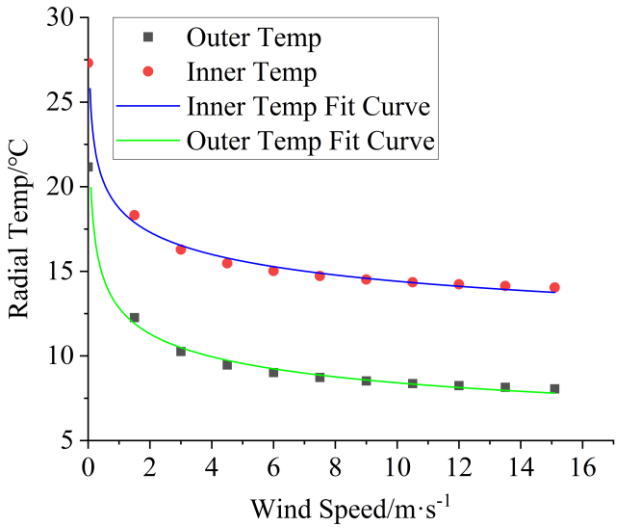

(a) Radial Temperature of Overhead Conductor

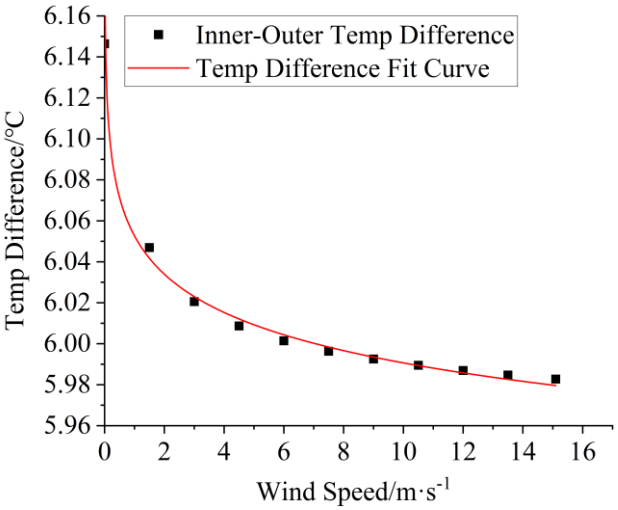

(b) Temperature Difference Between Inner and Outer Layers

Fig. 6 Radial Temperature Variation at Different Wind Speeds

3.4. Influence of Ambient Temperature on Radial Temperature Distribution of Overhead Conductors

To further discuss the impact of operating environmental temperature on the radial temperature distribution of overhead conductors, the temperature variation range of -19.6℃ to 33.7℃ in Xining in 2021 was used as the influencing factor [25]. The radial temperature changes of the overhead conductor within this temperature range were analyzed. The basic parameters for the temperature field in this calculation were the same as those in Section 2.2, and the wind speed was taken as the annual average value of 2.6 $m \cdot s^{-1}$. The variations in the radial temperature of the overhead conductor and the temperature difference between the inner and outer layers with environmental temperature are shown in Fig. 7.

The calculations reveal the following:

1) The radial temperature of the innermost layer of the overhead conductor increases linearly with the rise in environmental temperature. The fitting function of this relationship is shown in Equation (15).

2) When the environmental temperature rises from -19.6℃ to 33.7℃, the innermost layer temperature of the overhead conductor increases from -10.05℃ to 44.17℃, with the innermost layer temperature rising by 1.01℃ for every 1℃ increase in environmental temperature.

3) The results in Figure 7(b) show that the relationship between environmental temperature and the temperature difference between the inner and outer layers of the overhead conductor is approximately linear.

The main reasons for these phenomena include:

1) In a high-temperature environment, the thermal equilibrium state between the conductor and the environment may change. The conductor might absorb more heat and fail to dissipate it effectively, leading to heat accumulation inside the conductor and a resulting overall linear increase in its radial temperature.

2) At higher environmental temperatures, the air density decreases, reducing the efficiency of convective heat transfer. This decrease in heat exchange between the conductor and the surrounding air causes the temperature difference between the inner and outer layers to remain at a lower level due to the difficulty in dissipating the heat accumulated inside the conductor.

The fitting function formulas for the inner and outer layer temperatures based on different ambient temperatures are as follows:

$$Y_t = A + BX_{et} \tag{16}$$

where X_{et} represents the ambient temperature. The coefficients for the outer layer are: A = (3.8919 ± 0.0034) °C, B = (1.01584 ± 0.00019); The fitting coefficients for the inner layer: $A`$ = (9.9048 ± 0.0038) °C, $B`$ = (1.0175 ± 0.00021)。

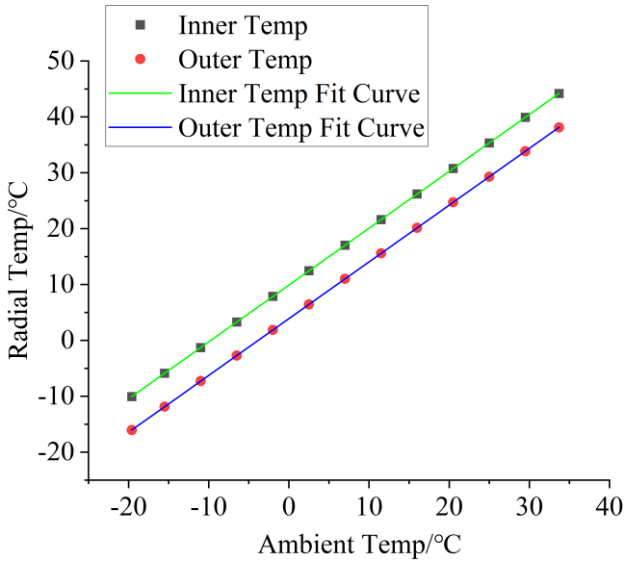

(a) Radial Temperature of Overhead Conductor

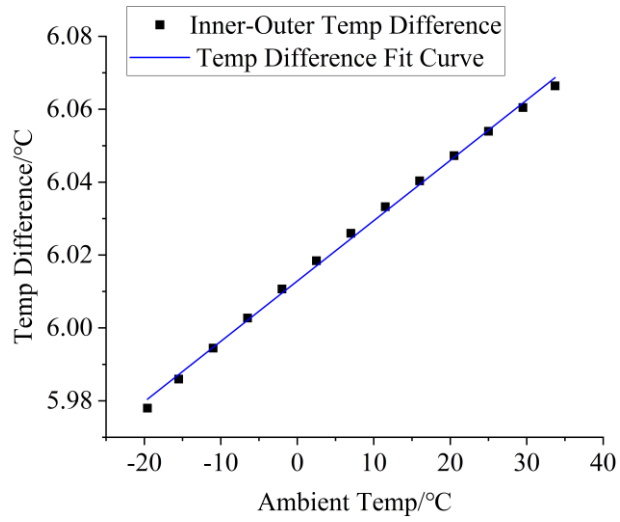

(b) Temperature Difference Between Inner and Outer Layers

Fig. 7 Radial Temperature Distribution at Different Ambient Temperatures

4. CONCLUSIONS

By applying the two-dimensional steady-state heat conduction equation, this paper establishes a numerical analysis method for iteratively simulating the radial temperature distribution of overhead conductors. Using the heat-resistant steel-cored aluminum stranded wire NRLH58GJ630-55 as an example, the radial temperature field distribution of this overhead conductor under plateau climate conditions is studied. The paper discusses the variation patterns of the temperature field of the overhead conductor with changes in wind speed, ambient temperature, and current on the Qinghai-Tibet Plateau. Based on the numerical calculation results under various working conditions, the following conclusions are drawn:

1) The temperature difference within the same layer of strands is negligible, and the radial temperature of the overhead conductor shows a trend of being higher inside and lower outside, with a significant temperature difference between the innermost and outermost layers.

2) As the current increases, the temperature of the overhead conductor and the temperature difference between the inner and outer layers both increase quadratically.

3) As the wind speed increases, as wind speed increases, the temperatures of the inner and outer layers of the overhead conductor decrease nonlinearly, and the reduction rate of their temperature difference slows down, exhibiting an exponential relationship.

4) With the increase in ambient temperature, the temperatures of the inner and outer layers of the overhead conductor exhibit a significant linear increase, while the temperature difference between the two layers remains relatively small.

REFERENCES

[1] National Meteorological Center. Wind Force Scale [Z]. General Administration of Quality Supervision, Inspection and Quarantine of the People's Republic of China; Standardization Administration of China. 2012: 8.

[2] ZHANG, Y. – ZHANG, L. – LI, G.: Investigation on Fire Accidents Caused by Single-Phase Tree-Ground Faults of 10 kV Overhead Lines [J]. Fire Science and Technology, 2022, 41(12):

[3] QIN, J. –NING, X. – FAN, S. et al.: Discharge ignition mechanism of tree-contacting single-phase-to-ground faults of overhead lines [J]. Power System Technology, 2023, 47(03): 1289-9

[4] LI, Y. – HAN, J. – HE, Ch. et al.: Study on lead wire breakage mechanism of a 750 kV UHV transmission line in strong wind zone [J]. Engineering Journal of Wuhan University, 2020, 53(10): 923-31.

[5] ZHANG, P. – ZHOU, S. – ZHENG, Z.: Analysis on strand breaking damage of overhead grounding wires with preventive measures [J]. Electric Power Safety Technology, 2022, 24(01): 67-8.

[6] WANG, X. – ZHENG, Q. – HUANG, G.: Research on the development of national standard for aeolian vibration fatigue test method of overhead conductors and cables [J]. Standard Science, 2022, (S1): 135-42

[7] LIU, G. – LI, Y. – CHEN, Y. et al.: Calculation and experiment verification on temperature distribution and radial temperature of overhead transmission line based on electromagnetic-thermal coupling fields [J]. Power System Protection and Control, 2018, 46(07): 7-13.

[8] DONG, X. – QU, F. – LI, Y. et al.: Construction of thermal conduction model for overhead conductor ampacity-temperature distribution under convection conditions [J]. Advanced Technology of Electrical Engineering and Energy, 2019, 38(01): 54-60.

[9] ZHANG, M. – LIANG, R. – ZHAO, G.: Study on Radial Temperature Distribution and Maximum Ampacity of Overhead Conductors [J]. Journal of Zhengzhou University (Engineering Science), 2020, 41(01): 1-7..

[10] LI, J. – JIA, S. – DU, D. et al.: Dynamic capacity analysis of overhead transmission lines considering temperature field [J]. Journal of Hunan University (Natural Sciences), 2020, 47(04): 57-66.

[11] BEŇA, Ľ, – GÁL, L. V. – KANÁLIK, M. et al.: Calculation of the overhead transmission line conductor temperature in real operating conditions [J]. Electrical Engineering, 2020, 103(2): 769-80.

[12] LIU, Z. – LI, H. – LIU, G. et al.: Analysis on radial temperature field of overhead conductor based on finite element simulation [J]. Insulating Materials, 2021, 54(03): 84-90.

[13] CUI, J. – ZHAO, L. – DAI, P. et al.: Online Monitoring Technique for Fatigue Damage of conductors Considering Temperature Difference Characteristics [J]. Guangdong Electric Power, 2023, 36(11): 96-105.

[14] ZHOU, H. – XIAO, K. – CHEN, Z. et al.: Numerical simulation on radial temperature distributions of operationaltransmission conductors [J]. Journal of Xiamen University (Natural Science), 2016, 55(01): 137-143.

[15] XIAO, K. – LIU, Y. – LI, P. et al.: Numerical analysis on temperature and stress filed coupling of overhead conductors [J]. Guangdong Electric Power, 2015, 28(11): 97-102.

[16] Shanghai Cable Research Institute. Concentric Lay Stranded Overhead Conductors of Circular Cross-Section [Z]. General Administration of Quality Supervision, Inspection and Quarantine of the People's Republic of China; Standardization Administration of China. 2017: 72.

[17] LIN, Q.: Analysis and application of non-contact dynamic capacity monitoring system for overhead line [J]. Inner Mongolia Electric Power Technology, 2023, 41(02): 81-5.

[18] AMES, W. F. – BREZINSKI, C.: Numerical methods for Engineers and Scientists[J].Mathematics and Computers in Simulation, 1992, 34(2):183-184.

[19] SAUER, T.: Numerical Analysis, 2nd Edition[J].[2024-07-26].

[20] LIU, Y. – CHEN, Z. – GU, Q.: Numerical algorithms for calculating temperature, layered stress, and critical current of overhead conductors[J]. Mathematical Problems in Engineering, 2020, 2020(1): 6019493.

[21] CIGRE. The thermal behavior of overhead conductors [R/OL]. 1992; 107-125. [2024-03-10]; http://www.ecigre.org/Publications/file.asp..

[22] PRICE, C. F. – GIBBON, R. R.: Statistical approach to thermal rating of overhead lines for power transmission and distribution[C]//IEE Proceedings C (Generation, Transmission and Distribution). IET Digital Library, 1983, 130(5): 245-256.

[23] NASA Goddard Earth Sciences (GES) Data and Information Services Center (DISC) (GES DISC MERRA2 - tavg1_2d_rad_Nx, https://disc.gsfc.nasa.gov/)

[24] National Bureau of Statistics of China. (2023). China Statistical Yearbook 2023. Retrieved from https://www.stats.gov.cn/sj/ndsj/2023/indexch.htm (Accessed on July 26, 2024).

[25] Qinghai Provincial Bureau of Statistics. (2023). Qinghai Statistical Yearbook 2023. Retrieved from http://tjj.qinghai.gov.cn/nj/2023/indexch.htm (Accessed on July 26, 2024).

ACKNOWLEDGMENTS

This paper was supported by the Qinghai Provincial Science and Technology Program (Youth) under the contract 2023-ZJ-962Q.

Received July 27, 2024, accepted September 26, 2024

BIOGRAPHIES

Hongwei Zhang was born in Zigong, Sichuan, received his bachelor's degree in Engineering in 2022. He is currently pursuing a master's degree in Civil and Hydraulic Engineering at Qinghai University. His research focuses on the numerical simulation of thermal-mechanical coupling problems in overhead conductors and experimental studies on wheel-rail friction issues.

Yongdou Liu was born in Xining, Qinghai, is the corresponding author of this paper. He graduated (MSc.) in Civil and Architectural Engineering from Xiamen University in June 2016. He obtained his PhD in Environmental Monitoring and Protection from Xiamen University in July 2021. His research focuses on the numerical simulation of thermal-mechanical coupling problems in overhead conductors and the dynamic response analysis of high-speed railway transportation systems.